Article

Not peer-reviewed version

Photoactive Hydrogels as Materials for Biological Applications Such as Antimicrobial Patches: Preparation of Thermally Stable Photoactive Films

Oscar Guillermo Marambio , Lidia Alvarez , Héctor Díaz-Chamorro , Julio Antonio Sanchez Poblete , Rudy Martin-Trasancos , Christian Erick Palavecino * , Guadalupe Del C. Pizarro *

Posted Date: 18 July 2025

doi: 10.20944/preprints202507.1501.v1

Keywords: bioinspired material; stimulus-response hydrogel films; biological applications; antimicrobial patches

 doi:10.20944/preprints202507.1501.v1

Article

Photoactive Hydrogels as Materials for Biological Applications Such as Antimicrobial Patches: Preparation of Thermally Stable Photoactive Films

Oscar G. Marambio [1], Lidia Álvarez [1], Héctor Díaz-Chamorro [1], Julio Sánchez [2], Rudy Martin-Trasancos [3], Christian Erick Palavecino [4,*] and Guadalupe del C. Pizarro [1,*]

[1] Departamento de Química, Facultad de Ciencias Naturales, Matemáticas y Medio Ambiente, Universidad Tecnológica Metropolitana (UTEM), J. P. Alessandri 1242. Santiago, Chile

[2] Departamento de Química Orgánica, Facultad de Química y de Farmacia, Pontificia Universidad Católica de Chile, Santiago, Chile.

[3] Departamento de Química de los Materiales, Facultad de Química y Biología, Universidad de Santiago de Chile (USACH), Santiago, Chile

[4] Laboratorio de Microbiología Celular, Centro de Ciencias Médicas aplicadas, Facultad de Medicina y Ciencias de la Salud, Universidad Central de Chile, Lord Cochrane 418, 8330546, Santiago, Chile

* Correspondence: christian.palavecino@ucentral.cl; gpizarro@utem.cl

Abstract

Hydrogel materials have emerged as an efficient, bioactive, and multifunctional alternative with significant potential for biomedical applications. This work aims to provide a valuable contribution to the design and implementation of stimulus-response films for optical processing and subsequently evaluate the usefulness of the photoactivity of the hydrogel films in photodynamic therapy (PDT) as antimicrobial patches. The design of stimulus-response polymeric hydrogel films is based on a hydrophilic polymer using vinyl monomers, 2-hydroxyethyl methacrylate (HEMA) and acrylamide (AAm) in molar ratios of 1:1 and the photochromic agent 3,3-dimethylindolin-6'-nitrobenzoespiropirano (BSP) for biological applications. The hydrogel films were prepared using the photoinitiator 2-hydroxy-4'-(2-hydroxyethoxy)-2-methylpropiophenone in the presence of a crosslinking agent, N, N'-methylene bisacryl amide (MBA) and ***BSP*** as a photoactive agent at different concentrations (0.1, 0.3, and 0.5 mol.%) to generate photoactive hydrogel films, which were subsequently used in biological photodynamic therapy (PDT). The PDT for *Staphylococcus aureus* using Ru(bpy) requires concentrations between 4 and 8 μg/mL to fully eliminate methicillin-sensitive strains (MSSA), while only partial inactivation is achieved for methicillin-resistant strains (MRSA). However, the incorporation of Ru(bpy) into a photoactive polymeric film containing the ***BSP*** significantly enhances its antimicrobial efficacy, reducing the minimum inhibitory concentration (MIC) to just 2 μg/mL for the complete inactivation of both strains. The new synergistic effect of BSP and Ru(bpy) confirm that these materials hold promise as next-generation antimicrobial coatings and innovative, light-sensitive materials.

Keywords: bioinspired material; stimulus-response hydrogel films; biological applications; antimicrobial patches

1. Introduction

Hydrogel materials have become one of the most popular materials depending on their application, such as contact lenses, oil recovery, pharmaceuticals, agriculture, textiles, and adherent materials [1–7]. They have emerged as an efficient bioactive multifunctional alternative [8–12]. These hydrogels can be cross-linked via thermal polymerization [13,14], photopolymerization [15,16], enzymatic crosslinking [17], and several other methods [18].

 doi:10.20944/preprints202507.1501.v1

The crosslinking process can be ionic or covalent and can change a macromolecule into solid or gel material by restricting its mobility [19]. Chemically cross-linked hydrogels are not reversible and have higher mechanical properties [19]. The strength of hydrogels can be attributed to different types of interactions, such as hydrogen bonds [20], ionic bonds [21], hydrophobic bonds [22,23], and hydrophilic bons [24,25].

The physicochemical properties of hydrogels can be easily modified, allowing them to be tailored for various biomedical applications. Hydrogel adhesive patches are widely used for transdermal drug delivery and have also found commercial applications. Beyond transdermal delivery, these hydrogel patches also have applications in cardiac therapy, cancer research, biosensing, and more [26–29].

Spiropyran is compatible with most polymerization conditions; therefore, it has been used with monomers, such as grafting onto preformed polymer chains. On the other hand, various approaches have been developed for spiropyran-linked polymers. The grafting approach has been employed to functionalize a variety of polymers, including polytetrafluoroethylene (PTFE) [30], polyaniline [31], polyacrylates [32], polysulfones [33], and polyphosphazenes [34,35].

Spiropyran (SP) is one of the most renowned hydrophobic photochromic compounds, photoisomerized to zwitterionic merocyanine (***MC***) by UV light irradiation. Merocyanine is then converted back to ***SP*** by visible light irradiation or heating. An essential property of ***MC*** is its ability to form metal ion complexes. The preparation of honeycomb films containing a photochromic ***SP*** moiety and the photopatterning of these films have been previously reported [36–39].

Therefore, some factors affect hydrogels' swelling ratio, such as chemical structure and composition of monomers [40,41], network structure [42], crosslinking ratio, and the specific stimuli or the surrounding medium [43,44]. Swelling and absorption properties of these materials are attributed to the presence of hydrophilic groups in the network [40]. For example, PHEMA has been employed in pharmaceutics and biomaterial applications [45,46]. Moreover, injuries caused by adhesive patches pose a significant threat to full-thickness skin trauma, as their strong adhesion can lead to severe pain and exacerbate the injury upon removal.

A work inspired by the mussel has been reported, in which an antibacterial hydrogel adhesive dressing has been designed and fabricated to care for wounds effectively. Unlike most difficult-to-remove dressings, this antibacterial adhesive hydrogel exhibited a substantial adhesion property, enabling painless and noninvasive on-demand removal within 2 seconds. The hydrogel also had excellent protein adsorption and mechanical, antibacterial, and biocompatibility properties [47,48].

In this sense, it is essential to highlight the potential application of these materials in biomedicine, particularly in the context of the rise of infections with bacteria resistant to conventional antimicrobial therapies.

The rise of multidrug-resistant (MDR) bacteria is one of the most pressing global health threats of the 21st century, significantly reducing the efficacy of current antimicrobial treatments. In the U.S., nearly 23,000 people die each year from antibiotic-resistant infections [49]. As resistance mechanisms continue to accumulate in bacteria, the number of effective therapeutic options steadily declines, underscoring the urgent need for alternative strategies. In this context, novel biomedical materials are being explored to complement conventional antibiotics and reduce MDR-related morbidity and mortality [50]. Among these alternatives, photodynamic therapy (PDT) offers the advantage of localized activation through light-based devices [51]. PDT combines a photosensitizer, oxygen, and light to generate reactive oxygen species (ROS), inducing non-specific photo-oxidative stress that inactivates bacteria. One particularly concerning MDR pathogen is *Staphylococcus aureus*, a Gram-positive bacterium responsible for approximately 30% of healthcare-associated infections (HAIs) [52–55]. MDR *S. aureus* strains are major contributors to HAIs such as surgical wound infections, urinary tract infections (UTIs), skin infections, and pneumonia [56–59]. This work aims to contribute to the design and preparation of thermally stable, solvent-resistant, photoactive honeycomb films as an antimicrobial patch for optical processing in biological applications, based on molecular and macromolecular components, and subsequently to evaluate the utility of photoactive polymers in

 doi:10.20944/preprints202507.1501.v1

photodynamic therapy (PDT). This work describes the design, synthesis, characterization, and application of a photoactive copolymer hydrogels derived from 2-hydroxyethylmethacrylate (HEMA) with acrylamide (AAm) monomers and the organic photosensitive compound 3,3-dimethylindoline-6′-nitrobenzospiropyran (***BSP***). The active polymeric hydrogel, poly(2-hydroxyethylmethacrylate-*co*-acrylamide), functionalized with ***BSP*** through physical interactions via a polymerization reaction. The optically active photoisomerizable spiropyran chromophore polymer is incorporated into the hydrogel, which is linked through physical interactions via the functional groups of the polymer chain.

Finally, we focused on determining its ability to inhibit the growth of methicillin-sensitive *S. aureus* (MSSA) as well as an MDR strain, the methicillin-resistant *S. aureus* (MRSA), both of which are the primary cause of superficial infections. This leads to the formation of a solid matrix that, when combined with a photosensitizer, facilitates its use in sanitary pads, hydrogels, or dressings that aid in treating or preventing superficial infections where light can easily activate the photosensitizer. The light-emitting properties of the polymers were characterized by the emission of blue and violet colors when exposed to UV light. They were subsequently used in an assay to verify their antimicrobial properties in photodynamic therapy (PDT). These macromolecular components exhibited an evident photon transfer process; based on this behavior, they were investigated with a photosensitizer molecule for PDT.

The photoactive hydrogel films were initially created using 2-hydroxy-4′-(2-hydroxyethoxy)-2-methylpropiofenone as a photoinitiator and N′N-methylene bisacrylamide (MBA) at different molar percentages as a cross-linking agent, along with 3,3-dimethylindoline-6′-nitrobenzospiropyran (***BSP***), via free radical polymerization in an aqueous solution. The polymer structure was designed based on a main chain with hydrophilic functional groups, which were functionalized through the incorporation of ***BSP***, allowing these materials to adapt to potential patch applications. This work introduces three significant contributions: (1) the functional groups of the hydrophilic hydrogel were used for functionalization with the photoactive, photochromic agent ***BSP***. The polymer's functional groups may enable the incorporation of ***BSP*** molecules through physical interactions such as hydrogen bonding and van der Waals forces; (2) the photoactive hydrogel films were prepared using a photoinitiator, with an equimolar ratio of monomers, cross-linking agent, and BSP in aqueous solution; and (3) The results indicate that during PDT, concentrations of 4 to 8 μg/mL of the photosensitizer Ru(bpy) are required to achieve complete inactivation of methicillin-sensitive *Staphylococcus aureus* (MSSA). In contrast, only a partial reduction in viability is observed for methicillin-resistant *S. aureus* (MRSA) strains. Notably, when the photoactive polymeric film containing the BSP matrix is used, the minimum effective concentration of Ru(bpy) is reduced by half to a quarter, achieving complete bacterial inactivation for both strains at just 2 μg/mL. This demonstrates that the hydrogel film enhances the photodynamic efficacy of the photosensitizer, effectively lowering its minimum inhibitory concentration (MIC). This improvement is likely due to the synergistic effect of the matrix, which may enhance local retention and stability of the photosensitizer, promote closer contact with bacterial cells, or facilitate more efficient local generation of reactive oxygen species.

Additionally, the material has good mechanical strength, thermal stability, and soft adhesive properties. The structural characterization was performed using FT-IR spectroscopy. Furthermore, the thermal and mechanical properties were measured, and the elastic properties of the hydrogels were quantified through mechanical tests (compressive and shear tests). Thermal analysis using thermogravimetric analysis (TGA) and differential scanning calorimetry (DSC) is carried out.

2. Results and Discussion

2.1. Synthesis and Characterization

The synthesis conditions of the poly(HEMA-*co*-AAm)-***BSP*** hydrogels and results are shown in Table 1.

 doi:10.20944/preprints202507.1501.v1

Table 1. Experimental conditions of the synthesis of poly(HEMA-*co*-AAm)-***BSP*** at 1:1 monomer ratios and different molar ratios of MBA and ***BSP*** (0.1, 0.3, and 0.5 mol.%).

Feed monomer ratio	[AAm] (mol/g)	[HEMA] (mol/g)	[MBA] (mol.-%)	[*BSP*] (mol.-%)	Yield (%)
P(HEMA-co-AAm) 1:1	0.015/1.065	0.015/1.950	0.0	0.0	95
P(HEMA-co-AAm) 1:1	0.015/1.065	0.015/1.950	0.1	0.0	90
P(HEMA-co-AAm) 1:1	0.015/1.065	0.015/1.950	0.3	0.0	90
P(HEMA-co-AAm) 1:1	0.015/1.065	0.015/1.950	0.5	0.0	92
P(HEMA-co-AAm) 1:1	0.015/1.065	0.015/1.950	0.1	0.1	90
P(HEMA-co-AAm) 1:1	0.015/1.065	0.015/1.950	0.3	0.3	90
P(HEMA-co-AAm) 1:1	0.015/1.065	0.015/1.950	0.5	0.5	90

Irgacure 2959: 0.019 M; *N'N*-methylene bis-acrylamide cross-linker (MBA).

Accordingly, poly(HEMA-co-AAm) and copolymer-***BSP*** hydrogels always yielded higher than 90%.

2.2. Structural Characterization by FT-IR Studies of the Hydrogels

Figure 1a,b shows the FTIR spectra of the poly(HEMA-co-AAm)-***BSP*** hydrogels at a 1:1 monomer feed ratio with MBA/***BSP*** (0.1, 0.3, and 0.5 mol.%, respectively). The FTIR spectra for the copolymer and poly(HEMA-co-AAm)-***BSP*** reveal changes in signal intensity for the HEMA groups after functionalization with BSP, as seen in Table 2. This can be explained by alterations in the individual peaks of –OH, –NH_2, –$CONH_2$, and –NO_2 groups. FTIR spectroscopy displayed bands in the range of 3200–3600 cm^{-1}, attributed to the stretching of the hydroxyl (–OH) and –NH deformation of the amide group; at 2847–2948 cm^{-1}, related to –CH stretching of methyl (–CH_3) and methylene (–CH_2–) groups; the band at 1713 cm^{-1} corresponds to the –C=O vibration of the ester group from HEMA; at 1665 and 1610 cm^{-1} attributed to ester groups of ***BSP***; and at 1640–1680 cm^{-1} (C=O stretching, amide). The band at 1454 and 1422 cm^{-1} is assigned to the nitro symmetric –NO_2 from the ***BSP*** moiety, 1335 cm^{-1} (symmetric stretch Ar-NO_2);.1510 cm^{-1} (asymmetric stretching Ar-NO_2); and 1930-1836 cm^{-1} (Ar-H aromatic overtones). See Figure 1.

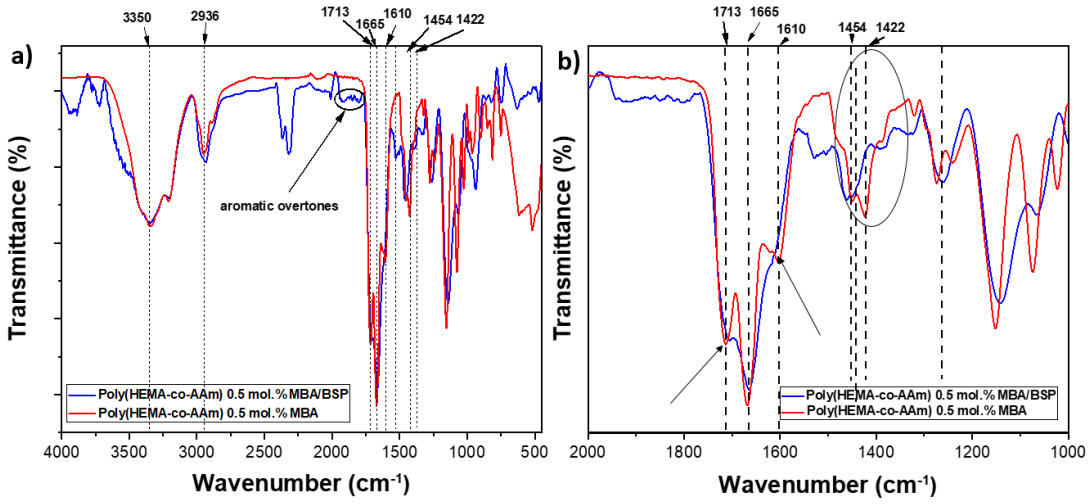

Figure 1. a) FT-IR spectrum of copolymer and P(HEMA-co-AAm)-BSP, b) Wavenumber ranges 2000-1000 cm^{-1}.

 doi:10.20944/preprints202507.1501.v1

Table 2 summarizes the leading vibration bands in the FT-IR spectra for the copolymers with and without ***BSP*** functionalization. Absorption bands in the IR spectra of the carbonyl tension bands from HEMA and ester groups have different intensities, which can generally be referred to as strong (s), medium (m), weak (w), broad, and sharp.

Table 2. Main vibration bands of the ***BSP***-functionalized copolymers.

	AAm	HEMA	Ester	-NO_2
Copolymer	(C=O)	(C=O)	(C=O)	-N-O
P(HEMA-*co*-AAm) 0.1 mol.% MBA	1658	1713 (s)	(w)	---
P(HEMA-*co*-AAm)-***BSP*** with 0.1 mol.% MBA	1659	(w)	1613 (s)	1454 (s)
P(HEMA-*co*-AAm) 0.5 mol.% MBA	1656	1713 (s)	(w)	---
P(HEMA-*co*-AAm)-***BSP*** with 0.5 mol.% MBA	1657	(w)	1610 (s)	1454 (s)

This variation in relative intensity of signals can be attributed mainly due to hydrogen bonding interaction between the two polymeric chains with functional ***BSP*** groups. The formation of physical attraction forces between hydrophilic functional groups (amide and hydroxyl groups) can significantly impact the intensity variations in an infrared (IR) signal [60], see Figure 2.

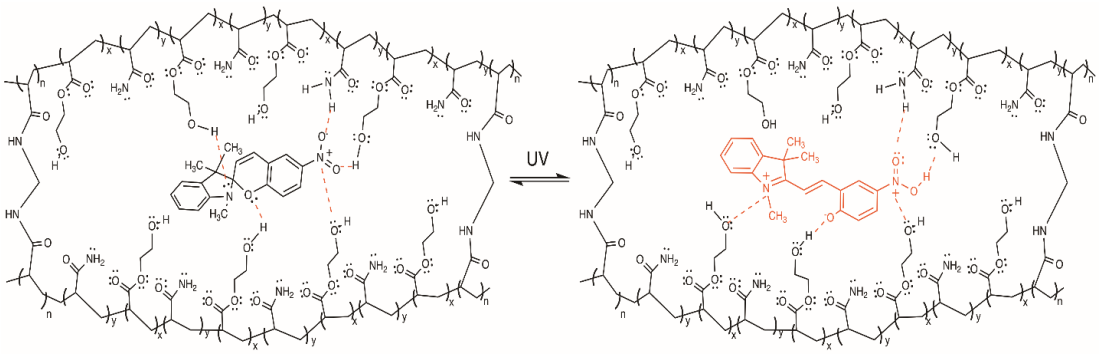

Figure 2. Schematic representation of the polymerization reaction of P(HEMA-co-AAm)-***BSP*** hydrogels.

2.3. Characterization by TGA and DSC

The TGA analysis of hydrogels at 1:1 feed ratio monomer with 0.1 and 0.5 mol.% MBA and 0.1 and 0.5 mol.% MBA/***BSP*** exhibited similar thermal decomposition, in general presented two-step degradations, see Figure 3a. The hydrogel at 0.5 mol.-% MBA exhibited the highest thermal stability with a residual loss mass percentage of 18% for the hydrogel, with extrapolated thermal decomposition temperatures, such as TDT_1 at 261.6 °C and TDT_2 at 349.5 °C. The hydrogels presented similar thermal behavior, but exhibited a greater thermal stability for the 0.5 mol.-% MBA in study.

 doi:10.20944/preprints202507.1501.v1

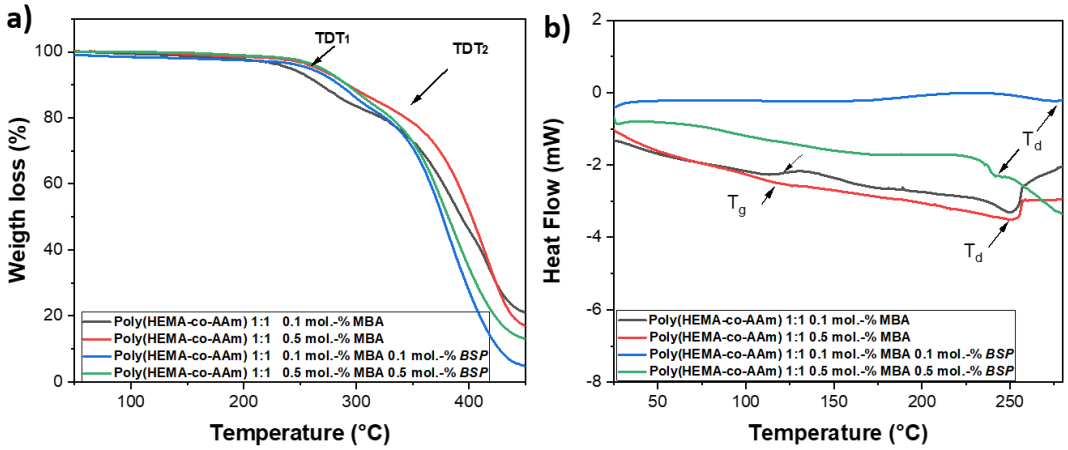

Figure 3. a) Thermograms and b) DSC curves of P(HEMA-co-AAm) and P(HEMA-co-AAm)-***BSP*** at 1:1 feed ratio monomer compositions and 0.1 and 0.5 mol.-% MBA and ***BSP***.

Furthermore, the results obtained from the DSC curve after the 2nd heating showed the formation of amorphous polymers with pronounced glass transition temperatures (Tg) at 0.1 and 0.5 mol.-% MBA and at 0.1 and 0.5 mol.-% MBA/***BSP***. At the same time, the curve DSC of the hydrogels exhibited a second event during heating, an endothermic peak, indicating the presence of a decomposition reaction (Td) of the material, which confirms the information provided by the TGA analysis. see Figure 3b. On the other hand, the Tg value at 0.1 mol.-% MBA is slightly lower but more pronounced, indicating a greater free volume in the hydrogel cells and greater movements of the functional groups and chains. The Tg value increases at a concentration of 0.5 mol.% MBA and less pronounced, indicating more restricted movements of the chains and functional groups due to the higher percentage of cross-linking. Tg values were found at 119.2 and 121.4 ± 0.1 °C, respectively. The results indicated that the hydrogels exhibit higher Tg value at higher mol.% MBA than for polymer chain [61], influenced by the reticulation reaction [62,63]. On the other hand, in the hydrogels functionalized with ***BSP***, the Tg is not evident, indicating a less flexible system, that is, a more rigid one. The presence of BSP, inserted between the polymer's backbones, decrease the interaction between these later, and hence decreases the thermal stability of the entirely hydrogel matrix. Additionally, support the result obtained by FTIR and confirms that BSP is in the hydrogel matrix interacting with the polymers, mainly through hydrogen bond interaction.

2.4. Swelling Behavior

Figure 4 shows the swelling behavior of the hydrogels at 0.1, 0.3, and 0.5 mol.-% MBA/***BSP*** The hydration capacity of poly(HEMA-*co*-AAm)-***BSP*** hydrogels was performed as a function of pH (pH = 3, 7, and 10). The swelling of the hydrogels increased with pH, where the maximum swelling is observed at pH 10. This is attributed to the reinforcement of H-bonding interaction of the carboxylate ($-COO^-$) functional groups with water. In addition, the swelling behavior increased over time; however, it eventually stabilized, achieving equilibrium. On the other hand, the percentage of hydration decreases as the percentage of crosslinking agent increases at 0.5 mol.% of MBA/***BSP***, as shown in Figure 4, probably due to the higher stiffness of the polymer matrix. It is important to stress that the presence of BSP don't affects as much as of the crosslinking degree, the swelling behavior of gels.

 doi:10.20944/preprints202507.1501.v1

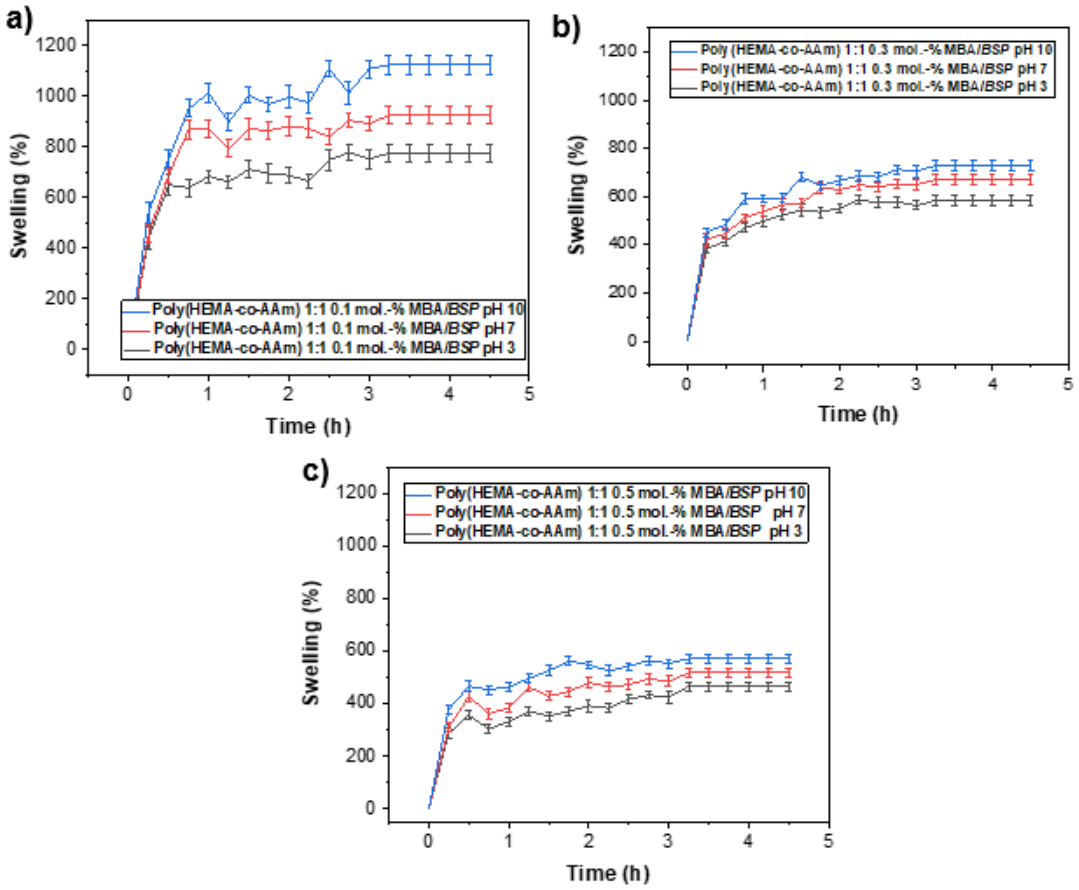

Figure 4. Hydration tests of the copolymer P(HEMA-co-AAm) 1:1 ratio with a) 0.1 mol.-% MBA, b) with 0.3 mol.-% MBA/***BSP***, c) 0.5 mol.-% MBA/***BSP***.

2.5. Mechanical Properties

The mechanical behavior of the poly(HEMA-*co*-AAm) hydrogels immersed in water at different feed monomer ratios and percentages of cross-linker MBA (mol.- %) has been studied. The mechanical properties of the hydrogels can be modulated based on the different kinds of technological applications [64–67]. The stress–strain curves of hydrogels are shown in Figure 4, whereas the Young modulus (E) (kPa) of the hydrogels are summarized in Table 3. The stress curves are plotted until the load applied reached 5 N. The reason is that some of the samples did not show a clear failure point.

Table 3. Effect of MBA and ***BSP*** at 0.1 and 0.5 mol.-% on the mechanical properties of the poly(HEMA-co-AAm) and poly(HEMA-co-AAm)-***BSP*** hydrogels at 1:1 feed ratio monomers.

Feed monomer ratio	MBA (mol.-%)	*BSP* (mol.-%)	Shear stress (kPa)	Shear modulus (kPa)
P(HEMA-co-AAm) 1:1	0.1	0.0	0.67 ± 033	1.69 ± 0.46
	0.5	0.0	1.97 ± 0.25	3.33 ± 1.27
P(HEMA-co-AAm)-***BSP*** 1:1	0.1	0.1	1.81±0.37	4.34 ±0.91
	0.5	0.5	3.41±0.17	6.18 ±1.02

 doi:10.20944/preprints202507.1501.v1

Lap Shear Test of Polymeric Hydrogel

Lap shear strength testing measures the ability of a material to withstand stresses set in a plane, where the exerted shear force is moving the two substrates in opposite directions. The test consists of loading a specimen comprising of a 3-ply laminate: substrate/polymer/ substrate.

The hydrogel with feed monomer ratios of 1:1 at 0.1 mol.-% MBA displayed less stiffness but with a lower resistance to failure, see Table 3. Moreover, the hydrogel with 1:1 feed monomer ratios at 0.5 mol.-% MBA sustained higher tension of failure shear, that is, a more excellent shear resistance against the applied force in wet conditions, the failure shear stress increases.

These results indicate that the 1:1 feed monomer ratio at 0.5 mol.% MBA/***BSP*** have higher failure shear stress and exhibit better adhesive properties. It can be suggested that in this study, we designed and synthesized an adhesive hydrogel that relies on dynamic interactions between functional groups and the hydrophilic substrate. Unlike most hydrogels, which can be challenging to remove, this adhesive hydrogel exhibits soft adhesion properties, allowing for the gentle and non-invasive removal of potential patch applications. Table 4 presents some results obtained for biological applications, which are compared with the findings from this work.

Table 4. Adhesive hydrogel biofilms and antibacterial abilities.

Polymeric materials	Biomedical application	Young modulus (E)*	References
Hydroxyethyl methacrylate –co-acrylamide with Dopamine	Catechol-based bioinspired adhesive properties in a wet medium	33.37±2.74-58.86±2.04 kPa	[23]
Maleic anhydride-modified β-cyclodextrin (CD), amantadine as a competitive guest	Adhesive antibacterial hydrogel	37.4-85.8 37.6 kPa	[47]
Chitosan grafted with methacrylate, dopamine, and N-hydroxymethyl acrylamide	Biofilm-inspired adhesive antibacterial hydrogel	34.0 kPa	[68]
Carboxymethyl chitosan hydrogel	Biodegradable carbohydrate polymers	2.3 kPa to 13.3 kPa, 12.5 kPa	[69]
Allyl cellulose with Dopamine	Mussel-inspired cellulose-based adhesive hydrogel	38.8 to 40.2 kPa	[70]
Hydroxyethyl methacrylate –co-acrylamide with cross-linker (MBA)	Biomimetic adhesive hidrogel	1.39 ± 0.06 kPa, 3.85 ± 1.87 kPa	[71]
Hydroxyethyl methacrylate with acrylamide, *N'N*-methylene bis-acrylamide (MBA) and photochromic agent (***BSP***)	Photoactive hydrogels as materials for biological applications, such as antimicrobial patches	4.34 ±0.91 6.18 ±1.02 kPa	This work

Tensile and compressive testing.

2.6. Antimicrobial Properties Based on Photodynamic Therapy (PDT)

Uncontrolled bleeding and infection can lead to significant increases in mortality. Hydrogel sealants have garnered considerable attention for their ability to control bleeding. However, because interfacial water poses a formidable barrier to solid surface bonding, the challenge remains to identify

 doi:10.20944/preprints202507.1501.v1

a product that provides robust tissue adhesion while simultaneously offering anti-infective properties.

Inspired by the adhesion mechanism of the biofilm P(HEMA-co-AAm) [71] in the present work, we introduce a novel adhesive hydrogel based on a synthetic P(HEMA-co-AAm) and the photochromic agent, 3,3-dimethylindolin-6'-nitrobenzoespiropirano (***BSP***), in conjunction with the cross-linker agent MBA through a straightforward radical photopolymerization process. ***BSP*** was included in the adhesive polymer to incorporate the properties of both, essential adhesive hydrogel and optical component (***BSP***), with light UV-Vis stimulus-response properties, respectively. P(HEMA-co-AAm)-***BPS*** displayed adequate adhesion, between 4.34 ± 0.91 and 6.18 ± 1.02 kPa, and excellent antibacterial properties. Therefore, P(HEMA-co-AAm)-***BSP*** represents a promising class of biomaterials for hemostasis and wound healing with sufficient efficiency. Table 4 presents bioadhesive patches designed for use in wet environments (hemostatic) that have shown limited adhesion to moist tissue surfaces, with an adhesive strength of less than 40 kPa [23,47,68–72]. An ideal bioadhesive for wet conditions should be both rigid and elastic, allowing minimal resistance to the natural deformation of dynamic soft tissues such as skin, which ranges from 0.1 to 100 kPa [73,74].

We first evaluate the antimicrobial activity of the Ru(bpy) photosensitizer (PS) to decrease the viability of *S. aureus* bacteria. A liquid culture containing $1x10^7$ CFU/mL of *S. aureus* (both MRSA and MSSA) was exposed to 0 – 8 μg/mL of Ru(bpy) and activated with 17 μW/cm² of blue light at 450–460 nm for 10 minutes. Figure 5a shows that Ru(bpy) significantly reduces the bacterial viability of MSSA by 6 $\log_{10}$ at 2 μg/mL ($p < 0.01$). For MRSA at 2 μg/mL, bacterial viability was reduced by 3 $\log_{10}$ ($p < 0.05$). Higher concentrations of Ru(bpy) significantly reduce the bacterial viability of the MSSA strain, achieving complete inactivation at concentrations ranging from 4 to 8 μg/mL, but not for the MRSA strain.

To preserve the photodynamic properties of the Ru(bpy) photosensitizer when embedded in the photoactive P(HEMA-coAAm)-***BSP*** hydrogel, the matrix was polymerized at the bottom of 24-well plates. The photosensitizer in aqueous solution was then applied as a thin layer over the photoactive hydrogel matrix at concentrations ranging from 0 to 8 μg/mL. The layer was left for 30 minutes to allow the Ru(bpy) photosensitizer to embed into the photoactive hydrogel matrix. S. aureus strains MRSA and MSSA were inoculated onto the matrix at 1×10^7 CFU/mL, incubated in the dark for 10 minutes, and samples were collected. Next, the plate was illuminated with blue light at 17 μW/cm² at 450–460 nm for 10 minutes to activate the PS, and samples were again collected. As shown in Figure 5b, the photoactive P(HEMA-coAAm)-***BSP*** hydrogel with Ru(bpy), which was not exposed to light, showed no antimicrobial activity compared to the control. Conversely, the irradiated plate showed increased antimicrobial activity, as seen in Figure 5c, achieving complete inactivation of MSSA and MRSA with 2 μg/mL of Ru(bpy), reducing the bacterial viability by 7 $\log_{10}$. This rise in photodynamic activity may be due to the hydrogel matrix's optical properties. When a photosensitizer in its ground state (S) absorbs light, it transitions to the excited singlet state (1S*). This short-lived state quickly undergoes intersystem crossing with the photoactive hydrogel to form a more stable, longer-lived triplet excited state (3S*). In this state, the photosensitizer can initiate two types of photosensitized oxidation pathways, called type I and type II reactions. In type I pathways, 3S* may participate in electron transfer or, less often, generate radicals or radical ions [75]. These radicals can undergo subsequent electron transfer reactions. In type II pathways, 3S* transfers energy to ground-state molecular oxygen, producing $^1O_2$. Since energy transfer from the triplet sensitizer to triplet oxygen is spin-allowed, it is highly favored in the presence of oxygen, facilitating efficient production of $^1O_2$· [76,77]. Both the radicals from type I reactions and $^1O_2$ generated in type II reactions can oxidize biomolecules. The oxidation of membrane lipids by photosensitization is a key event that can lead to photodynamic cell death.

 doi:10.20944/preprints202507.1501.v1

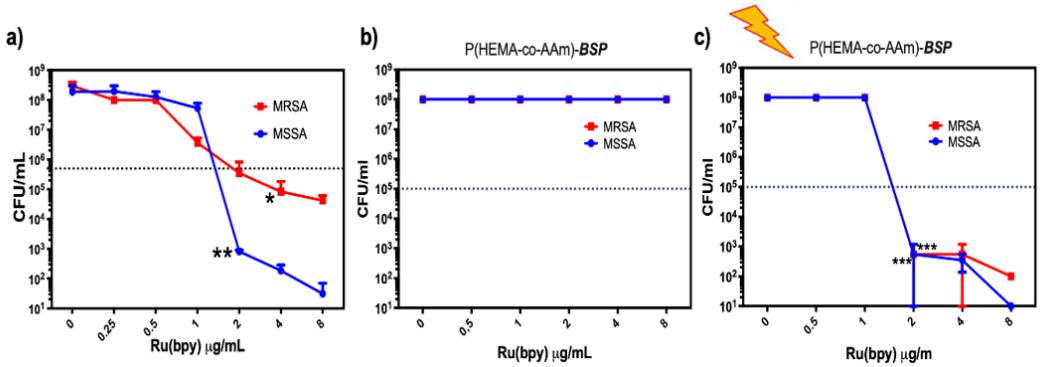

Figure 5. The photodynamic antimicrobial activity of the P(HEMA-co-AAm)-***BSP*** copolymer in combination with the Ru(bpy) photosensitizer. The photodynamic antimicrobial activity against methicillin-susceptible (MSSA) and methicillin-resistant (MRSA) *Staphylococcus aureus* was assessed: the MIC of the photosensitizer Ru(bpy) was determined between 0 and 8 µg/mL (a), the intrinsic antibacterial activity of P(HEMA-co-AAm)-***BSP*** was evaluated in the dark (b), and the reduction in MIC for P(HEMA-co-AAm)-***BSP*** and PS activated by light was assessed by embedding 0 - 8 µg/mL Ru(bpy) in the P(HEMA-co-AAm)-***BSP*** matrix (c). Bacterial viability is expressed as the $\log_{10}$ of the mean ±SD, with * $p < 0.05$ and ** $p < 0.01$ from a two-tailed t-test with comparison to control bacteria in the dark.

3. Conclusions

A new series of photoactive polymer hydrogels, designed as materials for biological applications, such as antimicrobial patches in wet environments, has been developed and characterized. Changes in the intensity of the carbonyl peak of functional groups were observed with a with a variation in signal intensities at 1713 cm^{-1} and 1610 cm^{-1}. This variation in the intensities is attributed mainly to the formation of physical forces attraction between the functional groups and the photoactive active agent generating forces of van der Waals and hydrogen bonds with the amine and the hydroxyl groups.

On the other hand, the hydrogels exhibited high thermal stability, as observed in TGA and DSC analysis. Concerning mechanical properties, these results indicate that the 1:1 feed monomer ratio at 0.5 mol.% MBA/***BSP*** have higher failure shear stress and exhibit better adhesive properties. It can be suggested that in this study, we designed and synthesized an adhesive hydrogel that relies on dynamic interactions between functional groups and the hydrophilic substrate. This result can also be attributed to a certain degree of physical interaction, mainly due to the formation of hydrogen bonds between the –OH functional group.

The ability of this matrix to preserve photodynamic activity was evaluated using the well-known photosensitizer Ru(bpy). Although Ru(bpy) exhibited photodynamic antimicrobial activity against *Staphylococcus aureus*, it was significantly effective against the MSSA strain on its own, showing a dose-dependent reduction in bacterial load, which increased in the presence of the photoactive P(HEMA-co-AAm)-***BSP*** hydrogel. In contrast, the Ru(bpy) efficacy against the MRSA strain was limited, as even higher concentrations of the photosensitizer failed to reduce bacterial viability by more than 4 log10. Notably, when embedded in the photoactive matrix, Ru(bpy) not only retained its photodynamic antimicrobial activity but also demonstrated a marked improvement in efficacy against MRSA. Where the activity of 2 µg/mL significantly increases, reducing bacterial viability by 7 $\log_{10}$, this is comparable to that observed with MSSA. The photoactive P(HEMA-co-AAm)-BSP hydrogel with Ru(bpy), which was not exposed to light, showed no antimicrobial activity compared to the control. Conversely, the illuminated Ru(bpy) -polymeric matrix complex exhibited increased antimicrobial activity, reducing the viability of MSSA and MRSA.

This approach expands the potential applications of hydrogels as adhesive materials in wet conditions, particularly as biomaterials, with swelling properties suitable for bioinspired

 doi:10.20944/preprints202507.1501.v1

applications. This kind of material can be applied in biological areas where low water absorption is needed.

4. Experimental

4.1. Reagents

Chemicals were used without further purification and were of analytical grade. Acrylamide (AAm, Aldrich CHEMIE, Germany) and 2-hydroxyethyl methacrylate (HEMA, 99% Merck, Germany) were used as the monomers. Benzoyl peroxide (BPO, 99.98 %, Sigma-Aldrich); 1,3,3-Trimethyl-2-methylen-indoline (97%, Sigma-Aldrich); 2-hydroxy-5-nitrobenzaldehyde (98 % Sigma-Aldrich), 2,3,3-trimethylindoline, 2-bromoethanol, 2-butanone, trimethylamine, 2-bromoethanol (C_2H_5BrO, Sigma-Aldrich), 2-butanone ($C_2H_5COCH_3$, 99.0%, Sigma-Aldrich), all *were commercially obtained from Sigma-Aldrich* (St. Louis, MO, USA). 2-hydroxy-4′-(2-hydroxyethoxy)-2-methylpropiofenone. (IRGACURE 2959, 99,5%, Merck, Germany) was used as a photoinitiator, and all analytical grades were pure grade. The *N′N*-methylene bisacrylamide (MBA, 99.5% Merck, Germany) was used as a crosslinking agent. All chemicals were used as received without further purification.

4.2. Measurement

The hydrogel samples' IR spectra were recorded at room temperature through PerkinElmer (USA) Fourier transform infrared (FTIR) Spectra 2000 using the attenuated total reflection ATR–FTIR method.

The TGA measurements were carried out at a heating rate of 10°C/min under nitrogen atmosphere with a flow rate: 150 cm^3 min^{-1}) by a thermogravimetric analyzer (TGA/DSC1 1100 SF, Mettler Toledo, Barcelona, Spain). The hydrogel sample size (between 3-4 ± 0.1 mg) were used in each experiment. The thermal analysis by differential scanning calorimetry (DSC) was carried out in a nitrogen atmosphere with a DSC Mettler Toledo 822e analyzer. The measurements were carried out at a heating rate of 10°C/min under nitrogen atmosphere with a flow rate: 50 cm^3 min^{-1}. All experiments were measure from 25 °C to 550 °C in an inert atmosphere (N_2 gas).

4.3. Synthesis of the 3,3-Dimethylindoline-6′-Nitrobenzospiropyran (BSP)

The synthesis was conducted in a 250 mL three-neck flask placed in an oil bath equipped with a magnetic stirrer and a condenser. To the flask, 4 mL (23 mmol) of 1,3,3-trimethyl-2-methylene-indoline and 4 g (23 mmol) of 2-hydroxy-5-nitrobenzaldehyde were added in 80 mL of ethanol. The mixture was heated to boiling at 78°C for 5 hours. Upon completion of the reaction, a dark green solid product was obtained, which was filtered and dried on filter paper in an oven for 72 h. The product obtained from the synthesis was purified by crystallization. Solubility tests were conducted using various solvents, including chloroform, ethanol, methanol, and acetone, which indicated that a 1:1 mixture of methanol and acetone showed improved solubility at elevated temperatures. In an Erlenmeyer flask equipped with a heating mantle, 50 mL of the 1:1 methanol and acetone solvent mixture was heated to boiling. The resulting product (solute) was then added, and the solvent mixture was gradually introduced in small amounts until the solid was completely dissolved. The Erlenmeyer flask was wrapped in absorbent paper to allow for slow cooling of the solution. It was covered with a watch glass to facilitate crystallization, which took place over a period of 96 hours. After this time, vacuum filtration was performed, followed by cold methanol washes. The final product obtained was a dark yellow or faintly brown crystalline solid, see Figure 6.

 doi:10.20944/preprints202507.1501.v1

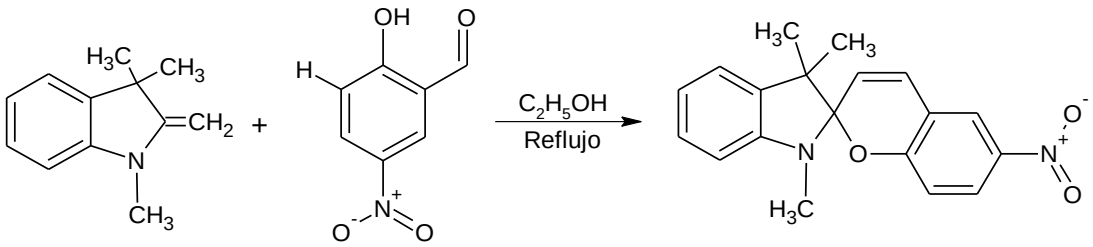

Figure 6. Reaction scheme for the synthesis of trimethylindoline-6-nitro-spirobenzopyran (***BSP***).

4.4. Hydrogel Films Preparation

The hydrogel films were prepared by free radical polymerization using an equimolar monomer feed ratio 1:1 (HEMA/AAm), in the presence of 2-hydroxy-4′-(2-hydroxyethoxy)-2-methylpropiophenone. (IRGACURE 2959) as photoinitiator, the cross-linker percentage (MBA), as cross-linker agent, and 1,3,3-trimethyl-2-methylene-indoline (***BSP***) as photochromic agent, based on a procedure previously reported by our group [23]. The polymerization reaction was carried out in aqueous solution using irradiation. A general method is described for 1:1 feed ratio monomer HEMA/AAm, 15 mmol of each monomer (50:50 mol-%), 0.5 mmol-% of IRGACURE 2959, MBA and ***BSP*** (at 0.1 and 0.5 mmol-%) were dissolved in 8 mL distilled water and 250 µL aliquot was added into sterile 24-wells cell culture plates. Subsequently, the mixture was exposed to UV radiation for three hours. The Poly(HEMA-*co*-AAm)-***BSP*** hydrogels were maintained sealed to maintain their hydration state. Finally, the dried hydrogels were characterized by Fourier Transform Infrared (FT-IR) spectroscopy, thermal properties, swelling behavior, and mechanical properties.

4.5. Swelling Studies

Swelling properties were investigated to develop absorbent polymers with suitable swelling properties for bio-applications.

The initial weight of the hydrogel samples was accurately measured after being freeze-dried. Then, the samples were immersed in a citrate buffer (pH<7) or phosphate buffer (pH >7) at 25°C and were swollen until the equilibrium state was reached. In this way, the dried samples of the copolymers were placed in a solution with a defined pH (3, 7, and 10). After specified time intervals, the swollen hydrogels were weighed after gently removing excess water using filter paper. The swelling ratio is defined using the following equation (Eq.1):

$$DS(\%) = \frac{(W_S - W_d)}{W_d} \times 100 \qquad \text{Eq. 1}$$

where *Ws* is the weight of the swollen hydrogel at an equilibrium state, and *Wd* is the weight of the dried hydrogel (Xerogel).

4.6. Lap Shear Test Studies

The objective of the shear test is to subject samples of the material to a state of shear stress. For this purpose, two portions of hydrogel are positioned between two cavities formed by three sandwiched plates of the assembly accessory. In an idealized way, each sample adopts a parallelepiped geometry with dimensions h=1mm, a=5mm and b= 5mm. Then, the assembly is rested in ambient conditions for 24 and later tested in a Cellscale 5000 biaxial tensile testing machine, equipped with a 10 N load cell, through movement relative between the plates in the longitudinal direction of the assembly. The shear stress in the reference configuration is calculated as $\tau = \frac{V}{A}$, where V is the shear force in one of the samples, which, given the double shear configuration, can be calculated as $V = \frac{F}{2}$, while A corresponds to the initial cut area $A = ab = 25mm^2$. Furthermore, the tangential deformation is calculated as $\gamma = \frac{\Delta}{h}$, where Δ corresponds to the relative displacement

 doi:10.20944/preprints202507.1501.v1

between jaws during the test. The adhesive strength was determined from the maximal loading over the area of the adhesive overlap. For the repeated adhesion tests, a waiting time of 10 min was needed before the next lap-shear cycle [64].

4.7. Determination of Antimicrobial Photodynamic Properties

The methicillin-sensitive MSSA and the methicillin-resistant MRSA *Staphylococcus aureus* strains were used for the assays. Bacteria were cultured in either solid or liquid Trypticase soy medium, as required. In a liquid medium, bacteria were grown to an optical density of $OD_{600\ nm}$ = 0.2–0.4. For photodynamic therapy (PDT), the bacteria were adjusted to 1 × 10^7 colony-forming units (CFU)/mL in a Phosphate-Buffered Saline (PBS) aqueous solution. The 1 x 10^7 UFC/mL bacteria were deposited in the wells of the 24-well plate over the P(HEMA-*co*-AAm)-***BSP*** hydrogels, with the photosensitizer Ru(bpy) [78] in various concentrations. Excitation was performed in a light box with 17 mW/cm² for 10 min using a blue LED lamp (450–460 nm), equivalent to 61.2 J/cm². After excitation, bacterial viability was determined by broth microdilution and colony counting on plates after 16–20 hours of incubation in Mueller–Hinton medium, as previously described [79]. Bacterial viability was expressed as the mean ± SD in CFU/mL. The MIC of the photosensitizer was determined by mixing 1 × 10^7 CFU/mL of bacteria with increasing concentrations of the photosensitizer Ru(bpy), between 0 and 8 μg/mL.

Acknowledgments: The authors gratefully acknowledge the support provided by FONDECYT grant numbers 1240357, 1231498, and 1241555. They also thank the Project funded by the Research Continuity Project Fund, year 2023, code PY LCLI23-02, Universidad Tecnológica Metropolitana.

Author Contributions: Conceptualization, O.M.; L.A., C.E.P and G.D.P.; methodology, L.A., C.E.P., H.D.C, and G.D.P.; software, L.A. H.D.C.; G.D.P.; resources, J.S. O.G.M and G.D.P.; writing—original draft preparation, R.M.T.; C.E.P. and G.D.P.; writing—review and editing, J.S. O.G.M.; C.E.P. and G.D.P.; visualization, O.G.M., R.M.T. C.E.P and G.D.P.; supervision, O.M., C.E.P and G.D.P. All authors have read and agreed to the published version of the manuscript.

Funding: This research received no external funding.

Institutional Review Board Statement: Not applicable.

Informed Consent Statement: Not applicable.

Conflicts of Interest: The authors declare no conflict of interest.

References

1. Vedadghavami, A.; Minooei, F.; Mohammadi, M. H.; Khetani, S.; Rezaei Kolahchi, A.; Mashayekhan, S.; Sanati-Nezhad, A. Manufacturing of Hydrogel Biomaterials with Controlled Mechanical Properties for Tissue Engineering Applications. *Acta Biomater* **2017**, *62*, 42–63. https://doi.org/10.1016/j.actbio.2017.07.028.
2. Serra, L.; Doménech, J.; Peppas, N. A. Engineering Design and Molecular Dynamics of Mucoadhesive Drug Delivery Systems as Targeting Agents. *European Journal of Pharmaceutics and Biopharmaceutics*. March 2009, pp 519–528. https://doi.org/10.1016/j.ejpb.2008.09.022.
3. Mizrahi, B.; Weldon, C.; Kohane, D. S. Tissue Adhesives as Active Implants; 2010; pp 39–56. https://doi.org/10.1007/8415_2010_48.
4. Mandell, S. P.; Gibran, N. S. Fibrin Sealants: Surgical Hemostat, Sealant and Adhesive. *Expert Opin Biol Ther* **2014**, *14* (6), 821–830. https://doi.org/10.1517/14712598.2014.897323.
5. Sangeetha, N. M.; Maitra, U. Supramolecular Gels: Functions and Uses. *Chem Soc Rev* **2005**, *34* (10), 821–836. https://doi.org/10.1039/b417081b.
6. Zhang, J.; Wang, A. Study on Superabsorbent Composites. IX: Synthesis, Characterization and Swelling Behaviors of Polyacrylamide/Clay Composites Based on Various Clays. *React Funct Polym* **2007**, *67* (8), 737–745. https://doi.org/10.1016/j.reactfunctpolym.2007.05.001.

 doi:10.20944/preprints202507.1501.v1

7. Wu, L.; Liu, M.; Rui Liang. Preparation and Properties of a Double-Coated Slow-Release NPK Compound Fertilizer with Superabsorbent and Water-Retention. *Bioresour Technol* **2008**, *99* (3), 547–554. https://doi.org/10.1016/j.biortech.2006.12.027.
8. Wang, Y.; Chen, G.; Zhang, H.; Zhao, C.; Sun, L.; Zhao, Y. Emerging Functional Biomaterials as Medical Patches. *ACS Nano* **2021**, *15* (4), 5977–6007. https://doi.org/10.1021/acsnano.0c10724.
9. Hwang, I.; Kim, H. N.; Seong, M.; Lee, S.; Kang, M.; Yi, H.; Bae, W. G.; Kwak, M. K.; Jeong, H. E. Multifunctional Smart Skin Adhesive Patches for Advanced Health Care. *Adv Healthc Mater* **2018**, *7* (15). https://doi.org/10.1002/adhm.201800275.
10. Jiang, Y.; Zhang, X.; Zhang, W.; Wang, M.; Yan, L.; Wang, K.; Han, L.; Lu, X. Infant Skin Friendly Adhesive Hydrogel Patch Activated at Body Temperature for Bioelectronics Securing and Diabetic Wound Healing. *ACS Nano* **2022**, *16* (6), 8662–8676. https://doi.org/10.1021/acsnano.2c00662.
11. Lee, S.; An, S.; Ryu, Y. C.; Seo, S. H.; Park, S.; Lee, M. J.; Cho, S.; Choi, K. Adhesive Hydrogel Patch-Mediated Combination Drug Therapy Induces Regenerative Wound Healing through Reconstruction of Regenerative Microenvironment. *Adv Healthc Mater* **2023**, *12* (18). https://doi.org/10.1002/adhm.202203094.
12. Xie, G.; Zhou, N.; Du, S.; Gao, Y.; Suo, H.; Yang, J.; Tao, J.; Zhu, J.; Zhang, L. Transparent Photothermal Hydrogels for Wound Visualization and Accelerated Healing. *Fundamental Research* **2022**, *2* (2), 268–275. https://doi.org/10.1016/j.fmre.2021.10.001.
13. Wang, H.; Zhu, D.; Paul, A.; Cai, L.; Enejder, A.; Yang, F.; Heilshorn, S. C. Covalently Adaptable Elastin-Like Protein–Hyaluronic Acid (ELP–HA) Hybrid Hydrogels with Secondary Thermoresponsive Crosslinking for Injectable Stem Cell Delivery. *Adv Funct Mater* **2017**, *27* (28), 1–11. https://doi.org/10.1002/adfm.201605609.
14. Shin, J. Y.; Yeo, Y. H.; Jeong, J. E.; Park, S. A.; Park, W. H. Dual-Crosslinked Methylcellulose Hydrogels for 3D Bioprinting Applications. *Carbohydr Polym* **2020**, *238* (January), 116192. https://doi.org/10.1016/j.carbpol.2020.116192.
15. Brown, T. E.; Carberry, B. J.; Worrell, B. T.; Dudaryeva, O. Y.; McBride, M. K.; Bowman, C. N.; Anseth, K. S. Photopolymerized Dynamic Hydrogels with Tunable Viscoelastic Properties through Thioester Exchange. *Biomaterials* **2018**, *178*, 496–503. https://doi.org/10.1016/j.biomaterials.2018.03.060.
16. Zhou, Y.; Liang, K.; Zhao, S.; Zhang, C.; Li, J.; Yang, H.; Liu, X.; Yin, X.; Chen, D.; Xu, W.; Xiao, P. Photopolymerized Maleilated Chitosan/Methacrylated Silk Fibroin Micro/Nanocomposite Hydrogels as Potential Scaffolds for Cartilage Tissue Engineering. *Int J Biol Macromol* **2018**, *108*, 383–390. https://doi.org/10.1016/j.ijbiomac.2017.12.032.
17. Kim, S. H.; Kim, K.; Kim, B. S.; An, Y. H.; Lee, U. J.; Lee, S. H.; Kim, S. L.; Kim, B. G.; Hwang, N. S. Fabrication of Polyphenol-Incorporated Anti-Inflammatory Hydrogel via High-Affinity Enzymatic Crosslinking for Wet Tissue Adhesion. *Biomaterials* **2020**, *242* (January), 119905. https://doi.org/10.1016/j.biomaterials.2020.119905.
18. Wei, Q.; Duan, J.; Ma, G.; Zhang, W.; Wang, Q.; Hu, Z. Enzymatic Crosslinking to Fabricate Antioxidant Peptide-Based Supramolecular Hydrogel for Improving Cutaneous Wound Healing. *J Mater Chem B* **2019**, *7* (13), 2220–2225. https://doi.org/10.1039/c8tb03147a.
19. Mredha, M. T. I.; Pathak, S. K.; Tran, V. T.; Cui, J.; Jeon, I. Hydrogels with Superior Mechanical Properties from the Synergistic Effect in Hydrophobic–Hydrophilic Copolymers. *Chemical Engineering Journal* **2019**, *362*, 325–338. https://doi.org/10.1016/j.cej.2018.12.023.
20. Oveissi, F.; Naficy, S.; Le, T. Y. L.; Fletcher, D. F.; Dehghani, F. Tough and Processable Hydrogels Based on Lignin and Hydrophilic Polyurethane. *ACS Appl Bio Mater* **2018**, *1* (6), 2073–2081. https://doi.org/10.1021/acsabm.8b00546.
21. Chang, B.; Ahuja, N.; Ma, C.; Liu, X. Injectable Scaffolds: Preparation and Application in Dental and Craniofacial Regeneration. *Materials Science and Engineering R: Reports* **2017**, *111*, 1–26. https://doi.org/10.1016/j.mser.2016.11.001.
22. Stojkov, G.; Niyazov, Z.; Picchioni, F.; Bose, R. K. Relationship between Structure and Rheology of Hydrogels for Various Applications. *Gels* **2021**, *7* (4). https://doi.org/10.3390/gels7040255.
23. Romero-Gilbert, S.; Castro-García, M.; Díaz-Chamorro, H.; Marambio, O. G.; Sánchez, J.; Martin-Trasancos, R.; Inostroza, M.; García-Herrera, C.; Pizarro, G. del C. Synthesis, Characterization and Catechol-Based

 doi:10.20944/preprints202507.1501.v1

Bioinspired Adhesive Properties in Wet Medium of Poly(2-Hydroxyethyl Methacrylate-Co-Acrylamide) Hydrogels. *Polymers (Basel)* **2024**, *16* (2). https://doi.org/10.3390/polym16020187.

24. Ahearne, M.; Yang, Y.; Liu, K. Mechanical Characterisation of Hydrogels for Tissue Engineering Applications. *Tissue Eng* **2008**, *4* (January 2008), 1–16.
25. Oyen, M. L. Mechanical Characterisation of Hydrogel Materials. *International Materials Reviews* **2014**, *59* (1), 44–59. https://doi.org/10.1179/1743280413Y.0000000022.
26. George, B.; Bhatia, N.; Kumar, A.; A., G.; R., T.; S. K., S.; Vadakkadath Meethal, K.; T. M., S.; T. V., S. Bioinspired Gelatin Based Sticky Hydrogel for Diverse Surfaces in Burn Wound Care. *Sci Rep* **2022**, *12* (1), 13735. https://doi.org/10.1038/s41598-022-17054-w.
27. Swain, S.; Pratap Singh, A.; Yadav, R. K. A Review on Polymer Hydrogel and Polymer Microneedle Based Transdermal Drug Delivery System. *Mater Today Proc* **2022**, *61*, 1061–1066. https://doi.org/10.1016/j.matpr.2021.10.320.
28. Carter, P.; Narasimhan, B.; Wang, Q. Biocompatible Nanoparticles and Vesicular Systems in Transdermal Drug Delivery for Various Skin Diseases. *Int J Pharm* **2019**, *555*, 49–62. https://doi.org/10.1016/j.ijpharm.2018.11.032.
29. Kamei, M.; Matsuo, K.; Imanishi, H.; Hara, Y.; Quen, Y.-S.; Kamiyama, F.; Oiso, N.; Kawada, A.; Okada, N.; Nakayama, T. Transcutaneous Immunization with a Highly Active Form of XCL1 as a Vaccine Adjuvant Using a Hydrophilic Gel Patch Elicits Long-Term CD8+ T Cell Responses. *J Pharmacol Sci* **2020**, *143* (3), 182–187. https://doi.org/10.1016/j.jphs.2020.04.004.
30. Chung, D.; Ito, Y.; Imanishi, Y. Preparation of Porous Membranes Grafted with Poly(Spiropyran-containing Methacrylate) and Photocontrol of Permeability. *J Appl Polym Sci* **1994**, *51* (12), 2027–2033. https://doi.org/10.1002/app.1994.070511207.
31. Bardavid, Y.; Goykhman, I.; Nozaki, D.; Cuniberti, G.; Yitzchaik, S. Dipole Assisted Photogated Switch in Spiropyran Grafted Polyaniline Nanowires. *The Journal of Physical Chemistry C* **2011**, *115* (7), 3123–3128. https://doi.org/10.1021/jp110665j.
32. Moniruzzaman, M.; Sabey, C. J.; Fernando, G. F. Photoresponsive Polymers: An Investigation of Their Photoinduced Temperature Changes during Photoviscosity Measurements. *Polymer (Guildf)* **2007**, *48* (1), 255–263. https://doi.org/10.1016/j.polymer.2006.08.066.
33. Warshawsky, A.; Kahana, N.; Buchholtz, F.; Zelichonok, A.; Ratner, J.; Krongauz, V. *Photochromic Polysulfones. 1. Synthesis of Polymeric Polysulfone Carrying Pendant Spiropyran and Spirooxazine Groups*; 1995; Vol. 34. https://pubs.acs.org/sharingguidelines.
34. Allcock, H. R.; Kim, C. Photochromic Polyphosphazenes with Spiropyran Units. *Macromolecules* **1991**, *24* (10), 2846–2851. https://doi.org/10.1021/ma00010a032.
35. Raymo, F. M.; Tomasulo, M. Optical Processing with Photochromic Switches. *Chemistry – A European Journal* **2006**, *12* (12), 3186–3193. https://doi.org/10.1002/chem.200501178.
36. Lewis, S. M.; Harbron, E. J. Photomodulated PPV Emission in a Photochromic Polymer Film. *The Journal of Physical Chemistry C* **2007**, *111* (11), 4425–4430. https://doi.org/10.1021/jp0669759.
37. WANG, S.; YU, C.; CHOI, M.; KIM, S. A Switching Fluorescent Photochromic Carbazole–Spironaphthoxazine Copolymer. *Dyes and Pigments* **2008**, *77* (1), 245–248. https://doi.org/10.1016/j.dyepig.2007.03.005.
38. Tomasulo, M.; Yildiz, I.; Raymo, F. M. Nanoparticle-Induced Transition from Positive to Negative Photochromism. *Inorganica Chim Acta* **2007**, *360* (3), 938–944. https://doi.org/10.1016/j.ica.2006.07.029.
39. Zhu, M.-Q.; Zhu, L.; Han, J. J.; Wu, W.; Hurst, J. K.; Li, A. D. Q. Spiropyran-Based Photochromic Polymer Nanoparticles with Optically Switchable Luminescence. *J Am Chem Soc* **2006**, *128* (13), 4303–4309. https://doi.org/10.1021/ja0567642.
40. Hamidi, M.; Azadi, A.; Rafiei, P. Hydrogel Nanoparticles in Drug Delivery. *Adv Drug Deliv Rev* **2008**, *60* (15), 1638–1649. https://doi.org/10.1016/j.addr.2008.08.002.
41. Guilherme, M. R.; Reis, A. V.; Takahashi, S. H.; Rubira, A. F.; Feitosa, J. P. A.; Muniz, E. C. Synthesis of a Novel Superabsorbent Hydrogel by Copolymerization of Acrylamide and Cashew Gum Modified with Glycidyl Methacrylate. *Carbohydr Polym* **2005**, *61* (4), 464–471. https://doi.org/10.1016/j.carbpol.2005.06.017.

 doi:10.20944/preprints202507.1501.v1

42. Patachia, S.; Valente, A. J. M.; Baciu, C. Effect of Non-Associated Electrolyte Solutions on the Behaviour of Poly(Vinyl Alcohol)-Based Hydrogels. *Eur Polym J* **2007**, *43* (2), 460–467. https://doi.org/10.1016/j.eurpolymj.2006.11.009.
43. Peppas, N. A.; Bures, P.; Leobandung, W.; Ichikawa, H. Hydrogels in Pharmaceutical Formulations. *European Journal of Pharmaceutics and Biopharmaceutics* **2000**, *50* (1), 27–46. https://doi.org/10.1016/S0939-6411(00)00090-4.
44. Xiong, Z.C.; He, Ch.C.;Huang, X.; Xu, L.; Zhang, L.F.; Xiong, Ch. Preparation and Properties of Thermo-Sensitive Hydrogels of Konjac Glucomannan Grafted n-Isopropylacrylamide for Controlled Drug Delivery. *Iranian Journal of Polymer Science and Technology* **2007**.
45. Alvarez-Lorenzo, C.; Concheiro, A. Reversible Adsorption by a PH- and Temperature-Sensitive Acrylic Hydrogel. *Journal of Controlled Release* **2002**, *80* (1–3), 247–257. https://doi.org/10.1016/S0168-3659(02)00032-9.
46. Elisseeff, L. L. and J. *Injectable Hydrogels for Cartilage Tissue Engineering*; 2003.
47. Yang, M.; Tian, J.; Zhang, K.; Fei, X.; Yin, F.; Xu, L.; Wang, Y.; Li, Y. Bioinspired Adhesive Antibacterial Hydrogel with Self-Healing and On-Demand Removability for Enhanced Full-Thickness Skin Wound Repair. *Biomacromolecules* **2023**, *24* (11), 4843–4853. https://doi.org/10.1021/acs.biomac.3c00576.
48. Khutoryanskiy, V. V. Advances in Mucoadhesion and Mucoadhesive Polymers. *Macromol Biosci* **2011**, *11* (6), 748–764. https://doi.org/10.1002/mabi.201000388.
49. Lahsoune, M.; Boutayeb, H.; Zerouali, K.; Belabbes, H.; El Mdaghri, N. Prévalence et État de Sensibilité Aux Antibiotiques d'Acinetobacter Baumannii Dans Un CHU Marocain. *Med Mal Infect* **2007**, *37* (12), 828–831. https://doi.org/10.1016/j.medmal.2007.05.006.
50. Magiorakos, A.-P.; Srinivasan, A.; Carey, R. B.; Carmeli, Y.; Falagas, M. E.; Giske, C. G.; Harbarth, S.; Hindler, J. F.; Kahlmeter, G.; Olsson-Liljequist, B.; Paterson, D. L.; Rice, L. B.; Stelling, J.; Struelens, M. J.; Vatopoulos, A.; Weber, J. T.; Monnet, D. L. Multidrug-Resistant, Extensively Drug-Resistant and Pandrug-Resistant Bacteria: An International Expert Proposal for Interim Standard Definitions for Acquired Resistance. *Clinical Microbiology and Infection* **2012**, *18* (3), 268–281. https://doi.org/10.1111/j.1469-0691.2011.03570.x.
51. Liu, Y.-Y.; Wang, Y.; Walsh, T. R.; Yi, L.-X.; Zhang, R.; Spencer, J.; Doi, Y.; Tian, G.; Dong, B.; Huang, X.; Yu, L.-F.; Gu, D.; Ren, H.; Chen, X.; Lv, L.; He, D.; Zhou, H.; Liang, Z.; Liu, J.-H.; Shen, J. Emergence of Plasmid-Mediated Colistin Resistance Mechanism MCR-1 in Animals and Human Beings in China: A Microbiological and Molecular Biological Study. *Lancet Infect Dis* **2016**, *16* (2), 161–168. https://doi.org/10.1016/S1473-3099(15)00424-7.
52. Paczosa, M. K.; Mecsas, J. Klebsiella Pneumoniae: Going on the Offense with a Strong Defense. *Microbiology and Molecular Biology Reviews* **2016**, *80* (3), 629–661. https://doi.org/10.1128/MMBR.00078-15.
53. Ko, W.-C. Community-Acquired Klebsiella Pneumoniae Bacteremia: Global Differences in Clinical Patterns. *Emerg Infect Dis* **2002**, *8* (2), 160–166. https://doi.org/10.3201/eid0802.010025.
54. Lakhundi, S.; Zhang, K. Methicillin-Resistant Staphylococcus Aureus: Molecular Characterization, Evolution, and Epidemiology. *Clin Microbiol Rev* **2018**, *31* (4). https://doi.org/10.1128/CMR.00020-18.
55. Diekema, D. J.; Pfaller, M. A.; Schmitz, F. J.; Smayevsky, J.; Bell, J.; Jones, R. N.; Beach, M. Survey of Infections Due to *Staphylococcus* Species: Frequency of Occurrence and Antimicrobial Susceptibility of Isolates Collected in the United States, Canada, Latin America, Europe, and the Western Pacific Region for the SENTRY Antimicrobial Surveillance Program, 1997–1999. *Clinical Infectious Diseases* **2001**, *32* (s2), S114–S132. https://doi.org/10.1086/320184.
56. Podschun, R.; Ullmann, U. *Klebsiella* Spp. as Nosocomial Pathogens: Epidemiology, Taxonomy, Typing Methods, and Pathogenicity Factors. *Clin Microbiol Rev* **1998**, *11* (4), 589–603. https://doi.org/10.1128/CMR.11.4.589.
57. Nadasy, K. A.; Domiati-Saad, R.; Tribble, M. A. Invasive Klebsiella Pneumoniae Syndrome in North America. *Clinical Infectious Diseases* **2007**, *45* (3), e25–e28. https://doi.org/10.1086/519424.
58. Giulieri, S. G.; Tong, S. Y. C.; Williamson, D. A. Using Genomics to Understand Meticillin- and Vancomycin-Resistant Staphylococcus Aureus Infections. *Microb Genom* **2020**, *6* (1). https://doi.org/10.1099/mgen.0.000324.

 doi:10.20944/preprints202507.1501.v1

59. Zhang, R.; Wang, F.; Kang, J.; Wang, X.; Yin, D.; Dang, W.; Duan, J. *Prevalence of Multidrug Resistant Gram-Positive Cocci in a Chinese Hospital over an 8-Year Period*; 2015; Vol. 8. www.ijcem.com/.
60. Morita, S.; Kitagawa, K.; Ozaki, Y. Hydrogen-Bond Structures in Poly(2-Hydroxyethyl Methacrylate): Infrared Spectroscopy and Quantum Chemical Calculations with Model Compounds. *Vib Spectrosc* **2009**, *51* (1), 28–33. https://doi.org/10.1016/j.vibspec.2008.09.008.
61. Morita, S.; Ye, S.; Li, G.; Osawa, M. Effect of Glass Transition Temperature (Tg) on the Absorption of Bisphenol A in Poly(Acrylate)s Thin Films. *Vib Spectrosc* **2004**, *35* (1–2), 15–19. https://doi.org/10.1016/j.vibspec.2003.11.020.
62. Huang, C. W.; Sun, Y. M.; Huang, W. F. Curing Kinetics of the Synthesis of Poly(2-Hydroxyethyl Methacrylate) (PHEMA) with Ethylene Glycol Dimethacrylate (EGDMA) as a Crosslinking Agent. *J Polym Sci A Polym Chem* **1997**, *35* (10), 1873–1889. https://doi.org/10.1002/(SICI)1099-0518(19970730)35:10<1873::AID-POLA2>3.0.CO;2-P.
63. Singh, N. K.; Lesser, A. J. A Physical and Mechanical Study of Prestressed Competitive Double Network Thermoplastic Elastomers. *Macromolecules* **2011**, *44* (6), 1480–1490. https://doi.org/10.1021/ma1028054.
64. Normand, V.; Lootens, D. L.; Amici, E.; Plucknett, K. P.; Aymard, P. New Insight into Agarose Gel Mechanical Properties. *Biomacromolecules* **2000**, *1* (4), 730–738. https://doi.org/10.1021/bm005583j.
65. Buckley, C. T.; Thorpe, S. D.; O'Brien, F. J.; Robinson, A. J.; Kelly, D. J. The Effect of Concentration, Thermal History and Cell Seeding Density on the Initial Mechanical Properties of Agarose Hydrogels. *J Mech Behav Biomed Mater* **2009**, *2* (5), 512–521. https://doi.org/10.1016/j.jmbbm.2008.12.007.
66. Chan, E. S.; Lim, T. K.; Voo, W. P.; Pogaku, R.; Tey, B. T.; Zhang, Z. Effect of Formulation of Alginate Beads on Their Mechanical Behavior and Stiffness. *Particuology* **2011**, *9* (3), 228–234. https://doi.org/10.1016/j.partic.2010.12.002.
67. Choi, S. S.; Hong, J. P.; Seo, Y. S.; Chung, S. M.; Nah, C. Fabrication and Characterization of Electrospun Polybutadiene Fibers Crosslinked by UV Irradiation. *J Appl Polym Sci* **2006**, *101* (4), 2333–2337. https://doi.org/10.1002/app.23764.
68. Han, W.; Zhou, B.; Yang, K.; Xiong, X.; Luan, S.; Wang, Y.; Xu, Z.; Lei, P.; Luo, Z.; Gao, J.; Zhan, Y.; Chen, G.; Liang, L.; Wang, R.; Li, S.; Xu, H. Biofilm-Inspired Adhesive and Antibacterial Hydrogel with Tough Tissue Integration Performance for Sealing Hemostasis and Wound Healing. *Bioact Mater* **2020**, *5* (4), 768–778. https://doi.org/10.1016/j.bioactmat.2020.05.008.
69. Kłosiński, K. K.; Wach, R. A.; Girek-Bąk, M. K.; Rokita, B.; Kołat, D.; Kałuzińska-Kołat, Ż.; Kłosińska, B.; Duda, Ł.; Pasieka, Z. W. Biocompatibility and Mechanical Properties of Carboxymethyl Chitosan Hydrogels. *Polymers (Basel)* **2022**, *15* (1), 144. https://doi.org/10.3390/polym15010144.
70. Lu, S.; Zhang, X.; Tang, Z.; Xiao, H.; Zhang, M.; Liu, K.; Chen, L.; Huang, L.; Ni, Y.; Wu, H. Mussel-Inspired Blue-Light-Activated Cellulose-Based Adhesive Hydrogel with Fast Gelation, Rapid Haemostasis and Antibacterial Property for Wound Healing. *Chemical Engineering Journal* **2021**, *417*, 129329. https://doi.org/10.1016/j.cej.2021.129329.
71. Romero-Gilbert, S.; Díaz-Chamorro, H.; Marambio, O. G.; Sánchez, J.; Martin-Trasancos, R.; Inostroza, M.; García-Herrera, C.; Pizarro, G. del C. Influence of Different Experimental Conditions on Bond Strength of Self-Adhesive Synthetic Polymer System Hydrogels for Biological Applications. *React Funct Polym* **2025**, *213*, 106264. https://doi.org/10.1016/j.reactfunctpolym.2025.106264.
72. Engler, A. J.; Sen, S.; Sweeney, H. L.; Discher, D. E. Matrix Elasticity Directs Stem Cell Lineage Specification. *Cell* **2006**, *126* (4), 677–689. https://doi.org/10.1016/j.cell.2006.06.044.
73. Zheng, Y.; Shariati, K.; Ghovvati, M.; Vo, S.; Origer, N.; Imahori, T.; Kaneko, N.; Annabi, N. Hemostatic Patch with Ultra-Strengthened Mechanical Properties for Efficient Adhesion to Wet Surfaces. *Biomaterials* **2023**, *301*, 122240. https://doi.org/10.1016/j.biomaterials.2023.122240.
74. Nam, S.; Mooney, D. Polymeric Tissue Adhesives. *Chem Rev* **2021**, *121* (18), 11336–11384. https://doi.org/10.1021/acs.chemrev.0c00798.
75. Martinez, G. R.; Ravanat, J.-L.; Cadet, J.; Miyamoto, S.; Medeiros, M. H. G.; Di Mascio, P. Energy Transfer between Singlet ($^1\Delta_g$) and Triplet ($^3\Sigma_g^-$) Molecular Oxygen in Aqueous Solution. *J Am Chem Soc* **2004**, *126* (10), 3056–3057. https://doi.org/10.1021/ja039111z.

 doi:10.20944/preprints202507.1501.v1

76. Greer, A. Christopher Foote's Discovery of the Role of Singlet Oxygen [$^1O_2$ ($^1\Delta_g$)] in Photosensitized Oxidation Reactions. *Acc Chem Res* **2006**, *39* (11), 797–804. https://doi.org/10.1021/ar050191g.
77. Schmidt, R. Photosensitized Generation of Singlet Oxygen. *Photochem Photobiol* **2007**, *82* (5), 1161–1177. https://doi.org/10.1562/2006-03-03-lR-833.
78. Li, F.; Collins, J. G.; Keene, F. R. Ruthenium Complexes as Antimicrobial Agents. *Chem Soc Rev* **2015**, *44* (8), 2529–2542. https://doi.org/10.1039/C4CS00343H.
79. Hormazábal, D. B.; Reyes, Á. B.; Cuevas, M. F.; Bravo, A. R.; Costa, D. M.; González, I. A.; Navas, D.; Brito, I.; Dreyse, P.; Cabrera, A. R.; Palavecino, C. E. Photodynamic Effectiveness of Copper-Iminopyridine Photosensitizers Coupled to Zinc Oxide Nanoparticles Against Klebsiella Pneumoniae and the Bacterial Response to Oxidative Stress. *Int J Mol Sci* **2025**, *26* (9), 4178. https://doi.org/10.3390/ijms26094178.